ARTICLE NO. 79-0786R

J80-125

Stability of Circular Cylindrical Shells under Transient Axial Impulsive Loading

80006
80007

D. G. Zimcik*
Canadian FRAM Ltd., Chatham, Canada
and
R. C. Tennyson†
Institute for Aerospace Studies, University of Toronto, Toronto, Canada

A study was made of the buckling response of thin-walled circular cylindrical shells subjected to dynamic, transient, axial square-wave (stress) loading of varying time duration. Photoelastic plastic test models were investigated including both geometrically "near-perfect" and imperfect configurations. Using a nonlinear dynamic buckling anlaysis based upon the Donnell-Mushtari type shell equations, strains and radial deflections were obtained by means of a Galerkin procedure. Dynamic buckling loads were then estimated based upon the notion of a Southwell plot and comparisons made with experimental data. In addition, high-speed framing photography recorded the change in buckling mode isoclinic patterns to compare with analytical predictions. Nondimensional design graphs were also constructed illustrating dynamic buckling loads of shells for varying geometries and impact durations.

Nomenclature

c = $[3(1-\nu^2)]^{1/2}$
c_0 = $(E/\rho)^{1/2}$, one-dimensional wave speed
D = $Eh^3/12(1-\nu^2)$
E = modulus of elasticity
h = shell wall thickness
$K_1, \bar{K}_1, K_2$ = $\pi R/2\ell_{x1}q_0$, $\pi R/2\ell_{x2}q_0$, $2\pi R/\ell_y q_0$
ℓ_x, ℓ_y = axial and circumferential wavelengths, respectively
q_0 = $(R/h)^{1/2}[12(1-\nu^2)]^{1/4}$, classical axisymmetric buckling mode wave number
R = cylinder radius
t = time
$T_0^{(i)}$ = period of free vibration in ith mode
$= 2\pi R/c_0\,(16K_1^4+1)^{-1/2}$ (axisymmetric mode)

$$= (2\pi R)/c_0\left[(K_1^2+K_2^2)+\frac{K_1^4}{(K_1^2+K_2^2)^2}\right]^{1/2}$$

(asymmetric mode)
u, v, w = axial, circumferential, and radial displacements, respectively
$\bar{w}$ = initial radial shape imperfection
x, y, z = axial, circumferential, and radial coordinates, respectively
X, Y = xq_0/R and yq_0/R, respectively
δ = initial imperfection amplitude
ϵ = strain
λ = nondimensional load parameter
τ = pulse duration
μ = δ/h
ν = Poisson's ratio
ρ = density
σ = normal stress

Subscripts

cr = critical
$c\ell$ = classical
s = static
pps = pictures per second

Presented as Paper 79-0786 at the AIAA/ASME/ASCE/AHS 20th Structures, Structual Dynamics and Materials Conference, St. Louis, Mo., April 4-6, 1979; submitted May 7, 1979; revision received Nov. 1, 1979.

Index categories: Structural Dynamics; Structural Stability.

*Supervisor, Product Engineering.
†Professor. Member AIAA.

I. Introduction

THIN-walled circular cylindrical shells have constituted primary structural members in the aerospace industry for many years. Since structural stability is a major consideration in their design, a great deal of analytical and experimental work has been done to investigate their buckling behavior. This effort has led to a reasonably good understanding of their response to static loading, including the effects of initial shape imperfections, but dynamic axial loading is not as clearly defined.

Interest in dynamic loading developed with the advent of large multistage rockets and extraterrestrial landing vehicles in the early 1960's. This generated several analytical studies of the response of a circular cylindrical shell to a given dynamic load of various forms, the most common being the suddenly applied axial load of constant magnitude which is held indefinitely. The initial work on this subject by Roth and Klosner[1] and Budiansky and Hutchinson[2,3] deserves particular mention. Subsequently, several investigations[4-8] have expanded and extended this work to include various shell configurations. However, finite time loading has been given much less attention and except for the lower bound estimates of Ref. 3, no attempt has been made to show the effect of loading time duration on the dynamic buckling load for shells having a range of geometric imperfections. Few experimental data have been obtained and those reported[9-11] concerned only crudely made models similar to those which have led to very inconsistent results in static testing. However, one other experimental study[12] has shown good agreement with numerical results by employing a "ramp" loading whereby the load was increased rapidly at a constant rate until buckling occurred.

In general, designers have been reluctant to accept predicted buckling results until proved experimentally. The scope of the

present investigation was to determine analytically and experimentally the response of circular cylindrical shells to a suddenly applied axial load in the form of a "square-pulse," i.e., the load being raised very quickly to a given magnitude and maintained for a given time τ, and then released to zero very quickly. Both "geometrically perfect" and imperfect shells were tested on a specially designed and manufactured apparatus capable of providing loads of varying time duration to obtain the dynamic buckling value on first passage of the pulse as a function of both the imperfection and pulse duration. Two types of controlled initial shape imperfections were included: an axisymmetric distribution in the form of a "pure" trigonometric function in the axial direction ($\mu\cos KX$) and an asymmetric distribution of the form of a trigonometric function in each of the axial and circumferential directions ($\mu\cos K_1 X\cos K_2 Y$). This latter form of initial imperfection has been assumed to be present in almost all analytical investigations up to the present but has never been experimentally produced before.

II. Theoretical Analysis

The analytical treatment of this problem was based on the well-known Karman-Donnell large-deflection equilibrium equations, modified to include effects of initial shape imperfections and radial inertia, together with the corresponding compatibility equation.[1] For brevity, only an outline of the solution will be presented, the details of which can be found in Ref. 13.

Two equations were obtained in terms of the radial displacement and Airy stress function. These were solved using a Galerkin procedure to transform them into a set of coupled, time-dependent ordinary differential equations. The radial displacement function assumed for this purpose was similar in form to the initial geometric shape imperfection, which included terms in the form of the static buckling modes given by

$$\bar{w}(X,Y)=\bar{w}_1\cos 2\bar{K}_1 X+\bar{w}_{20}\cos 2K_1 X$$
$$+\bar{w}_{11}\cos K_1 X\cos K_2 Y+\bar{w}_{02}\cos 2K_2 Y \qquad (1)$$

It should be noted that this general form of the shape imperfection distribution was selected since it contains all of the fabricated initial imperfection shapes present in the test specimens.

The radial displacement function was assumed to be similar to the initial geometric shape imperfection including static buckling modes of the form

$$w(X,Y,t)=w_0(t)+w_1(t)\cos 2\bar{K}_1 X+w_{20}(t)\cos 2K_1 X$$
$$+w_{11}(t)\cos K_1 X\cos K_2 Y+w_{02}(t)\cos 2K_2 Y \qquad (2)$$

The inclusion of the two axisymmetric terms in both displacement functions has been shown in Ref. 12 to provide a necessary flexibility when investigating the behavior of shells with an axisymmetric shape imperfection whose wavelength differs greatly from the critical value ($\ell_{x_{cr}}=\pi R/q_0$).

It seems appropriate that some justification be given for the use of a displacement function which involves no axial motion with time to describe the deformation of a cylindrical shell subjected to a transient stress wave loading. For the shell specimens investigated, $\ell_{x_{cr}}$ (=axial buckle wavelength) was less than 2.5 cm, whereas the shortest input pulse length was 33 cm and increased to a maximum of 86 cm. Therefore, an axial section of the shell of sufficient length to form a ring of buckles around the circumference (i.e., one buckle wavelength) was subjected to a uniform compressive stress under the transient square-wave loading except for a short period of time at the start and end of the pulse. For the shortest pulse investigated, the time of uniform compressive stress was no less than 85% of the pulse duration and increased up to 95% for the longest pulse. Consequently, the response of the shell wall at any point could be approximated by considering the load to be applied or removed everywhere in the body at the same time.

The displacement function was capable of providing geometric continuity of the radial displacement in the circumferential direction but did not satisfy the axial edge constraint of the experiment at $x=0$. However, prebuckling bending effects are localized to a relatively small zone.

The focus of the present investigation was buckling on first passage of the input pulse. Therefore, no account was made for reflections of the stress pulse from the end of the shell. Analytically, the shell was assumed to be "very long" in order to neglect the effect of boundary conditions.

Substitution of the assumed displacement functions into the compatibility equation yields a solution for the Airy stress function. Since the displacement function is an approximation to the actual physical shell displacement, it does not satisfy the equilibrium equation exactly. The error involved is minimized by applying a Galerkin method to the equilibrium equation which results in a set of five time-dependent nonlinear ordinary differential equations that govern the radial deflection of the shell wall. These equations, together with the closure condition,[1,13] comprise a system of coupled, nonlinear ordinary differential equations with time-dependent displacements $w_0(t)\ldots w_{02}(t)$ whose solution was obtained by numerical integration. To simulate the passage of the stress pulse, the axial stress was increased at a predetermined rate (instantaneously for a perfect square-wave case) to a maximum value which was held for a given time τ (including rise time). The axial stress was then decreased at a predetermined rate to zero or a small residual value to simulate the experimental conditions. During this time, the growth in mode-amplitude coefficients was monitored together with the axial and circumferential surface strains (including bending) at successive small time increments. This sequence was repeated for increasing values of maximum input stress for each time duration τ in the domain of interest.

III. Experimental Methods

Dynamic Transient Axial Loading

Dynamic transient square-wave axial loading of the shell specimens was performed on an impact testing machine designed and constructed in the laboratory as shown in Fig. 1. A gas gun was used to propel a hardened steel projectile down at 2.5-m barrel to impact on the striker shell. The inside motion of the projectile was transferred to the striker shell by means of a steel piston attached by an aluminum cross-beam to an adjustable ring which contacted the striker shell. A restraint on the displacement of the piston ring assembly limited the contact time with the striker shell, which was then free to move in the axial direction on bearings to impact upon the test specimen that was also free to travel axially. After the event had been recorded, the test specimen was eventually brought to rest by an end stop. The design of the apparatus allowed for alignment of the striker and shell specimens to ensure uniform impact over the cross section.

The transient stress input to the shell specimen approximated a square-wave. An important feature which renders this machine unique was the independent control of time duration of loading τ and input stress magnitude σ, which were governed by the length of the striker cylinder and its velocity, respectively. Duration of loading ranged 200-450 μs, which physically corresponds to an input pulse of about 0.55-1.35 of the length of the shell specimen.

In the dynamic test apparatus, the specimen end condition approximated a simple edge support. The radial displacement at the end was restricted by friction during loading but the shell wall was relatively free to rotate. Friction also prevented circumferential displacements during loading. Axial displacement was limited in only one direction at the impacted

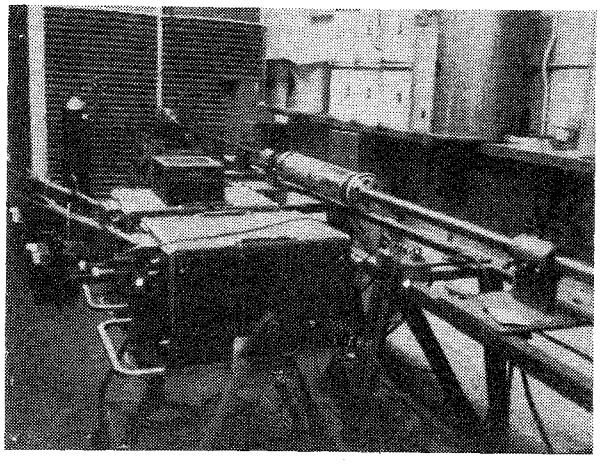

a) overall view

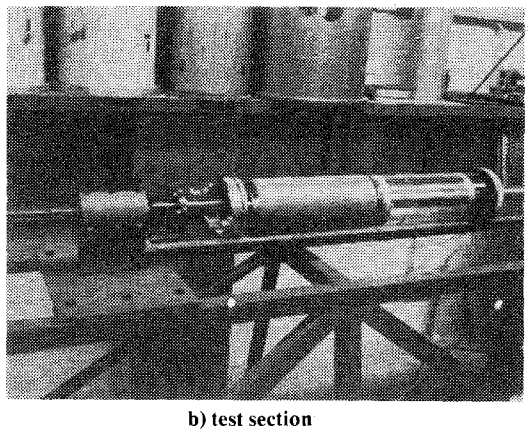

b) test section

Fig. 1 Dynamic square-wave axial loading apparatus.

end, while circularity of the specimen was maintained by the support bearings.

Fabrication of Shell Specimens

Geometrically "near-perfect" circular cylindrical shells were manufactured from a liquid epoxy plastic using the spin-casting technique.[14] Due to the material's high ratio of yield strength to modulus of elasticity, the shell models buckled entirely elastically and thus could be retested many times. In addition, this epoxy has been shown to behave in an almost linearly elastic manner for a wide range of dynamic loading.[15]

Geometrically imperfect cylindrical shell specimens were machined from a cylinder (spun-cast in a similar manner to the above) on a lathe using a hydraulic tracer tool apparatus and a suitable template. All specimens were of uniform thickness but contained a geometric shape imperfection in the form of an axisymmetric cosine function in the axial direction[16] or an asymmetric "checkerboard" pattern consisting of a cosine function of the axial coordinate modulated by a cosine function in the circumferential direction.

To fabricate asymmetric imperfections, a hydraulic tracer tool was made to follow a cylindrical template turning in a synchronous manner with a lathe head stock. The drive speed of the template was determined by the gear ratio between the driver on the face plate and the follower directly linked to the template. The circumferential imperfection frequency was determined by the speed of rotation of the template relative to the lathe turning speed, while the axial imperfection frequency and amplitude were determined by the template shape.

During the cutting process of the cylindrical steel bar template, its axis of symmetry was displaced from the axis of rotation of the lathe in a prescribed manner but always in the same plane. As detailed in Ref. 13, the end result was a cylinder of constant radius along its length but with the midpoint at any cross-section offset in one plane to approximate a cosine wave. When used in the shell imperfection profile cutting apparatus, any cross-section was seen as a circular cam against the tracer tool stylus which presented a true cosine in the circumferential direction.

Fabrication of Striker Shells

Design of a striker shell imposed the following requirements: a much stiffer wall than the test specimen to lessen the chance of generating transverse vibrations on impact; a much larger cross-sectional area to facilitate alignment of two shell bodies and to ensure uniform impact around the circumference of the test specimen; and finally, a linear density ratio of approximately one with respect to the test specimen for acoustical impedance matching. A sandwich construction using hollow honeycomb (Nomex) core between two thin facesheets of epoxy fulfilled all three requirements. The striker shells were also fabricated in the laboratory by a multistep procedure using the spin-casting apparatus.

Instrumentation

Because of the very short time durations of loading and the elastic behavior of the cylinders, it was not possible to observe buckling visually. Consequently, several small (0.159 cm) foil strain gages were bounded to the inner and outer cylinder surfaces and the dynamic strain histories were recorded on two dual-beam oscilloscopes which were triggered internally from the output of one gage mounted directly at the impacted end of the shell. A series of gages located 7.6 cm from the struck end at equal circumferential intervals were used to ascertain the uniformity of impact and also to determine buckling of the specimen by noting the appearance and subsequent rapid growth of bending components in strain as the striker shell impact velocity was increased.

High-Speed Framing Photography

To supplement the strain gage data, high-speed framing photography (using a 16 mm Hycam camera) recorded the deformation of the shell on impact for selected specimens at filming rates of 1500 ~ 6500 pps. The photoelastic technique was used in conjunction with the birefringent property of the epoxy to study the changing 22-½ and 45 deg isoclinics in the shell. A coating was applied to the inner wall of the cylinder by treating it with a volatile solution containing fine mesh aluminum powder to reflect the linearly polarized incident light.

Test Procedure

Because of the elastic behavior of the shells during loading, each specimen could be repeatedly tested to give reproducible results. The test procedure involved impacting the striker shell against the specimen at increasing velocity with each run. A series of response curves were thus obtained showing the strain as a function of time which were then used to define a dynamic buckling load for a given input pulse time duration. Each cylinder was subjected to a number of such sequences of varying time duration to outline the trend of the dynamic buckling loads.

IV. Discussion of Results

Shell Specimen Geometry

The geometric properties of each of the five shell specimens manufactured for this investigation are listed in Table 1. These include a "geometrically perfect" shell, three shells each containing an axisymmetric shape imperfection with differing spatial wavelength and amplitude, and one shell containing an asymmetric shape imperfection geometrically close to the static asymmetric buckling mode.

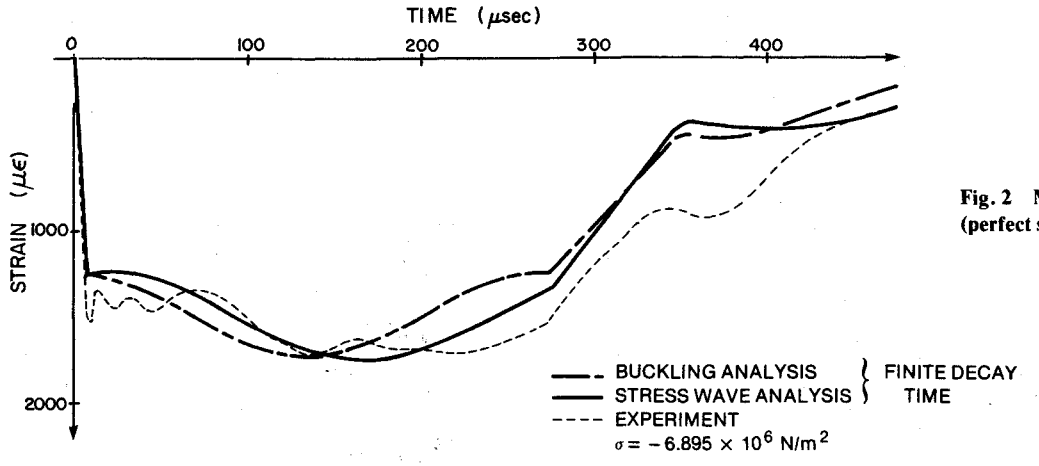

Fig. 2 Midsurface strain in axial direction (perfect shell).

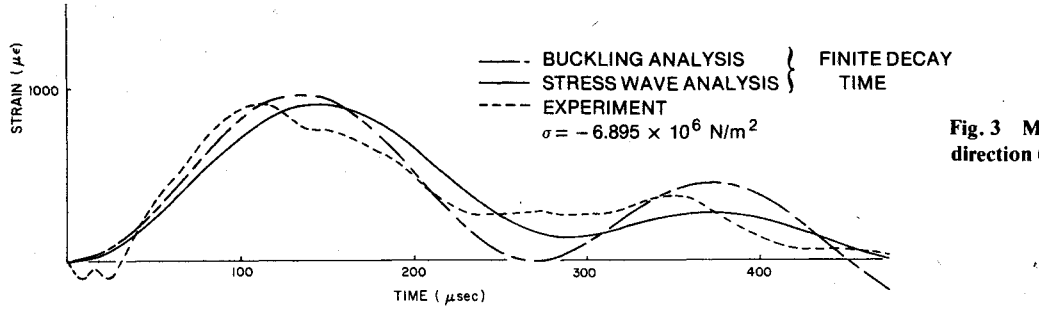

Fig. 3 Midsurface strain in circumferential direction (perfect shell).

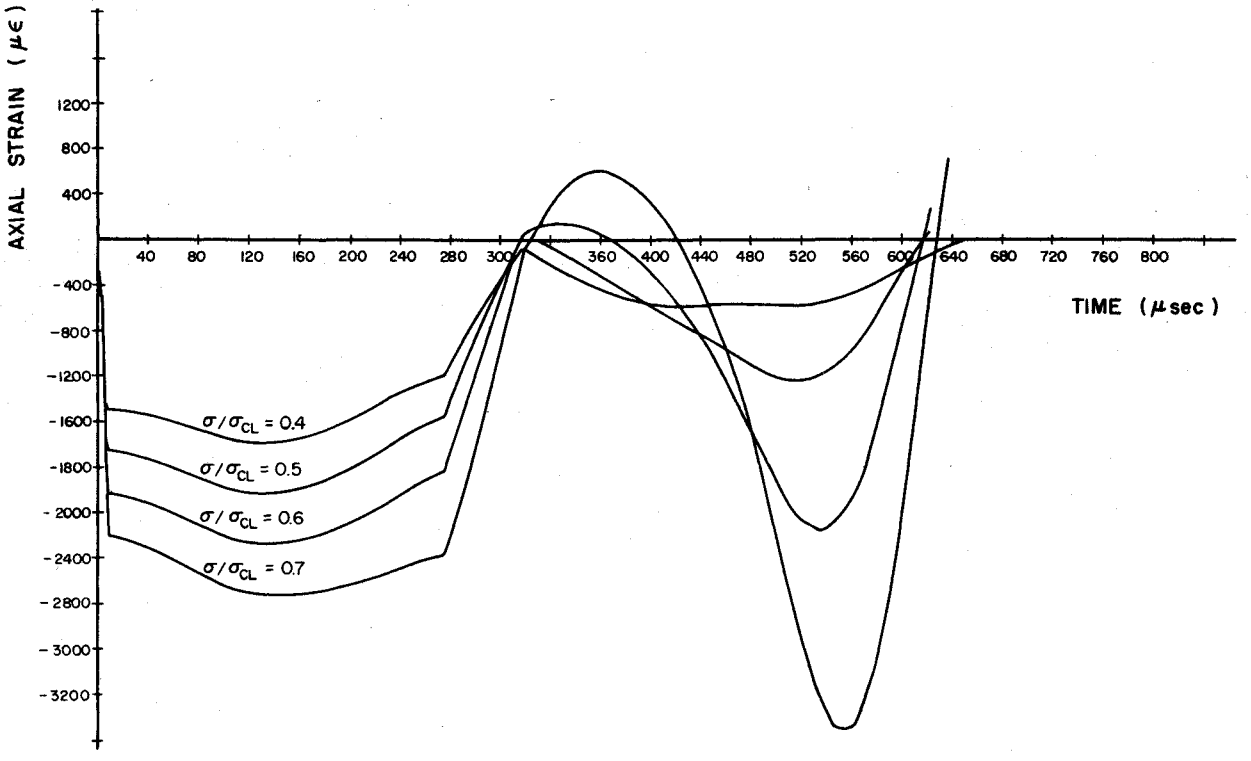

Fig. 4 Predicted strain gage traces for shell AS1 ($\tau = 275\ \mu s$).

Comparison of Buckling and Stress Wave Analyses

In order to compare directly with the experimental results, the output of the numerical solutions of the equations of motion for the buckling analysis (and a linear stress wave analysis, a description of which can be found in Ref. 13) provided values for the axial and circumferential strains in addition to the mode-amplitude coefficients as a function of time. Typical axial and circumferential strain gage outputs recording membrane strains are shown in Figs. 2 and 3 for the impact of a 27.9 cm striker shell with a "geometrically perfect" shell specimen. It can be seen that the axial strain output was not a square pulse because of the axial-radial displacement coupling of the shell wall. Due to the effects of dispersion and acoustical impedance mismatch at the contact

Table 1 Shell properties

Shell type	P "Perfect"	AX1 Axisymmetric imperfect	AX2 Axisymmetric imperfect	AX3 Axisymmetric imperfect	AS1 Asymmetric imperfect
R, cm	7.620	7.620	7.620	7.645	7.645
h, cm	0.0470	0.0622	0.0592	0.0635	0.0541
μ	—	0.0306	0.070	0.111	—
μ_1	—	—	—	—	0.159
K_1	—	0.517	0.680	0.176	—
K_1	—	—	—	—	0.470
K_2	—	—	—	—	0.472
ℓ_x, cm	—	1.174	0.871	3.500	2.413
ℓ_y, cm	—	—	—	—	4.801
$T_0^{(i)}$, μs	404	193	135	404[a]	429
$\sigma c\ell = Eh/Rc$, N/m^2	1.246×10^7	1.649×10^7	1.569×10^7	1.678×10^7	1.431×10^7
$\sigma_s/\sigma_{c\ell}$	1.0	0.754	0.733	0.786	0.555

[a] Due to imperfection wavelength, asymmetric mode dominates. $E\simeq3.21\times10^9$ N/m^2 dynamic value; $\nu=0.4$; $C_0\simeq1.676\times10^5$ cm/s.

surface, the input pulse had finite rise and decay times and after the passage of the pulse, there remained a residual stress. The magnitudes of these values were experimentally estimated to modify the pulse shape which was then used in the two analyses to produce the axial and circumferential strain curves shown. It would appear that the shell behavior on impact was adequately approximated by the analyses considered.

Comparison of Analysis and Experiment

From the buckling model analysis, it was found that when the axial load was removed after a time duration τ, the shell wall was generally left in a state of vibration (except when only one deformation mode was allowed and τ coincided exactly with the period of vibration). The magnitude of the wall vibration after loading was directly affected by the input stress magnitude for a given time duration of loading and was seen to be a linear sum of the deformation mode amplitudes with constant coefficients. This is particularly apparent in Fig. 4 which shows predicted axial outer surface strain-time profiles for increasing input stress levels for shell AS1. From these profiles, it was possible to measure a vibrational amplitude after loading and plot this data as a function of input stress.

Typical experimental outer surface axial strain-time curves for specimen AS1 subjected to increasing impact velocities are shown in Figs. 5a-c. These signals were from one gage only and contained both membrane and bending strain components. Such traces closely resemble those of Fig. 4 in shape and in particular show a similar nonlinear growth of vibrational amplitude at $t\approx500$ μs after impact. Measured values of vibrational amplitude from a series of such strain outputs at increasing input stress levels provided an experimental measurement of deformation magnitude for each combination of striker and specimen shell. The magnitude of the input stress was obtained in each case by graphical integration of the strain outputs for each run from a pair of strain gages mounted on the inner and outer wall surfaces. The data were used for comparing experiment and analysis for each of five striker shell lengths impacting five specimen shells. Approximately 10 data points were obtained for each pair, thus representing a total data set of over 500 strain-time records. Generally, the experimental data agreed very favorably with the analytical curves, as can be seen in Figs. 6-8. These results were obtained for geometrically "near per-

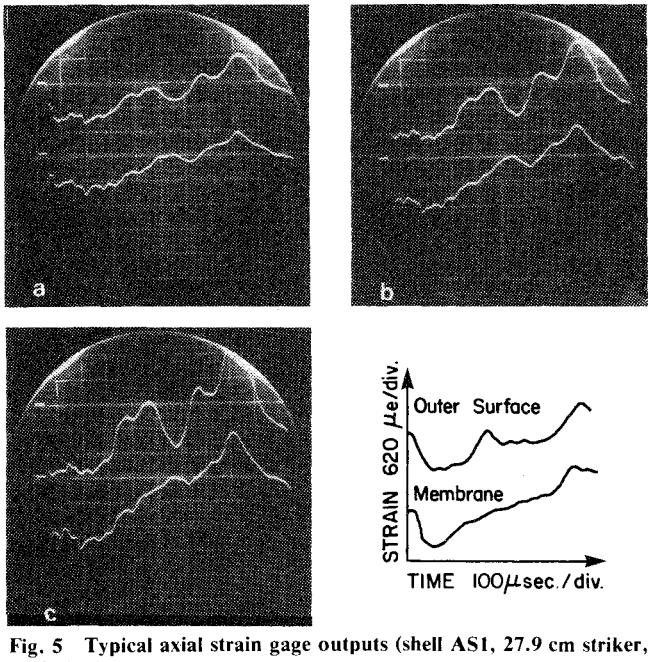

Fig. 5 Typical axial strain gage outputs (shell AS1, 27.9 cm striker, $\tau=275$ μs).

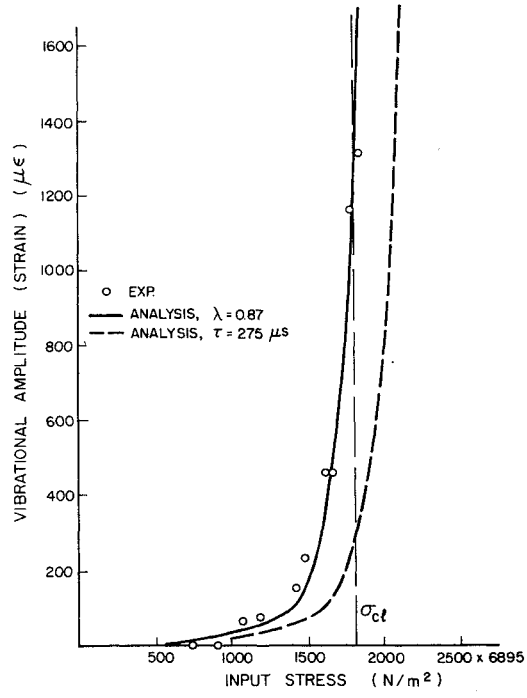

Fig. 6 Growth of vibrational amplitude with increasing stress ("perfect" shell, 27.9 cm striker).

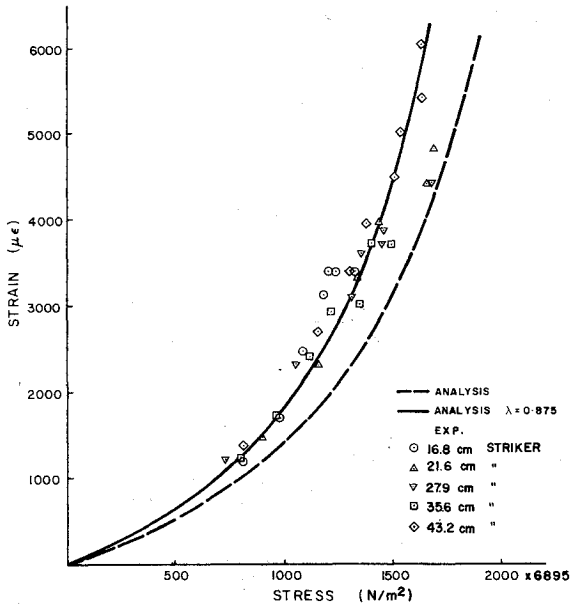

Fig. 7 Growth of vibrational amplitude during loading with increasing stress (shell AX2).

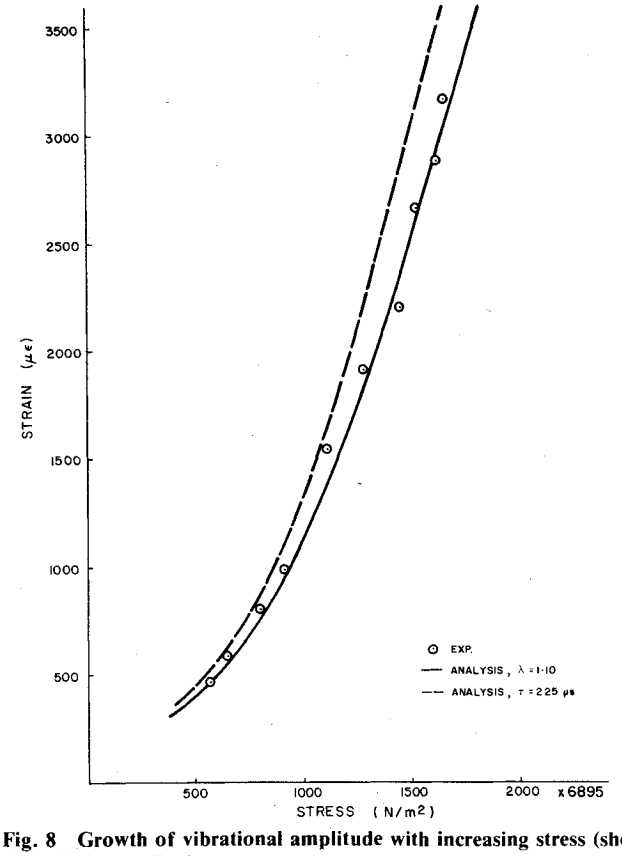

Fig. 8 Growth of vibrational amplitude with increasing stress (shell AS1, 21.6 cm striker).

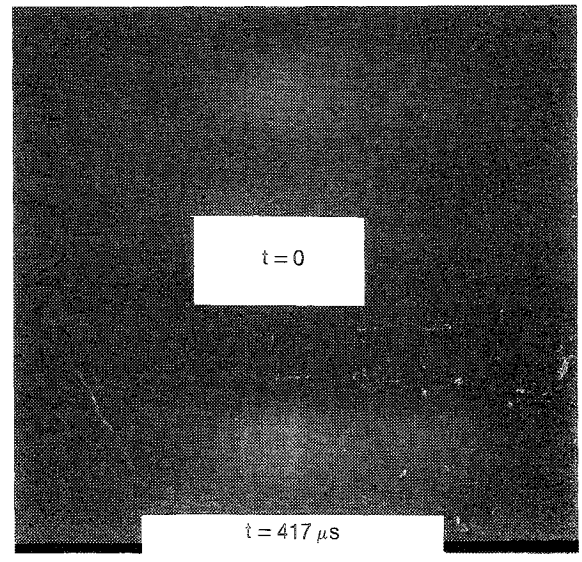

Fig. 9 High-speed photographs of 22-½ deg isoclinic patterns at impact for shell AX2.

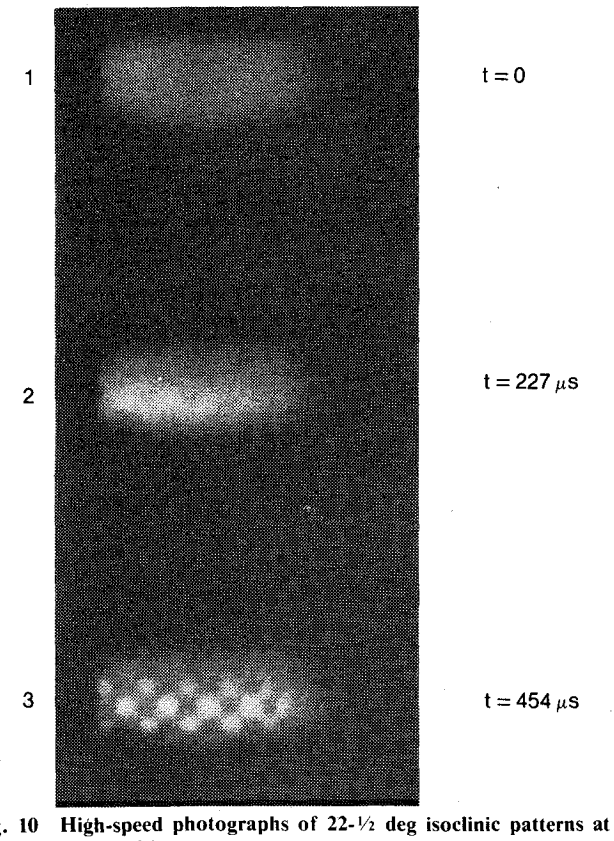

Fig. 10 High-speed photographs of 22-½ deg isoclinic patterns at impact for shell AS1.

fect," axisymmetric and asymmetric imperfect shells, respectively. Details of the test models' geometry and buckling stresses can be found in Table 1. Differences between the analytical curves and test data are attributed to the effects of boundary conditions, which approximated simple support ($u=v=w=\partial^2 w/\partial x^2=0$), and the assumed displacement function. Except for shells AX1 and AX2, all mode-amplitude coefficients continued to grow during the loading period, resulting in larger final values with longer loading times (τ). Therefore, measurement of the strain amplitude immediately after unloading gave an indication of the maximum value of deformation for the particular load and pulse duration. However, the other two shells (AX1 and AX2) containing axisymmetric shape imperfection wavelengths close to the static classical buckling mode value deformed in an entirely different manner. Analytically, deformation took place predominantly in the axisymmetric imperfection mode only (W_1), with negligible contributions arising from the other allowable modes. This mode amplitude oscillated with a frequency which was load dependent. It was also found for these two shells that this frequency was less than the shortest pulse duration of loading which was achieved due to limitations on striker shell lengths. As a

Table 2 Comparison of dynamic buckling mode wavelengths

Shell	Axisymmetric mode, cm		Asymmetric mode, cm		Ratio
	ℓ_x (measured)	ℓ_x (computed)	ℓ_x (measured)	ℓ_x (computed)	$\ell_x(m)/\ell_x(c)$
Perfect	2.057	2.108	—	—	0.98
AX2	1.803	1.753[a]	—	—	1.02
AX1	—	—	2.337	2.261	1.03

[a] Imperfection wavelength.

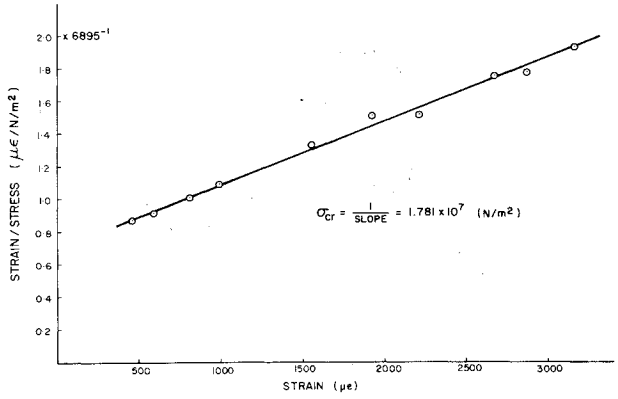

Fig. 11 Typical Southwell plot of experimental results for shell AS1 (21.6 cm striker).

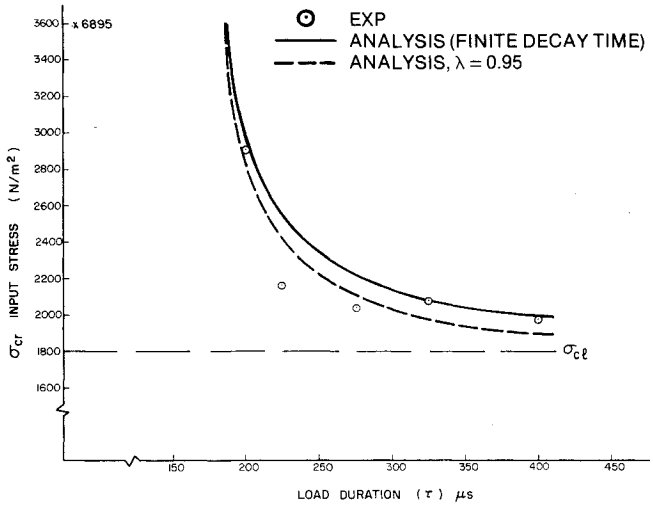

Fig. 12 Variation in buckling stress with load duration for "perfect" shell.

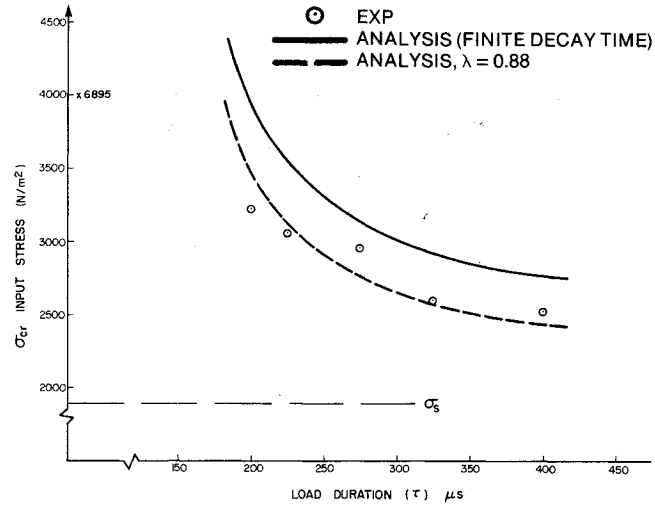

Fig. 13 Variation in buckling stress with load duration for shell AX3.

result, the test data obtained were independent of τ as can be seen in Fig. 7. However, in all cases, the experimental data exhibited similar behavior to the analytical results.

Buckling Modes

It is shown in Ref. 13 that axisymmetic deformation isoclinic patterns (for any angle other than 0, 45, or 90 deg) yield axisymmetric isoclinic rings and asymmetric deformation is indicated by a pattern of ovals whose shape depends on the mode wave numbers.

Photographs of the changing 22-½ deg isoclinic patterns for shell AX2 are shown in Fig. 9. Impact on the left end (in frame 2) produced dark axisymmetric rings over the shell containing the shape imperfections. These rings, indicating axisymmetric deformation, persisted in the imperfect half of the shell until an oval pattern spread from the right-hand ("perfect") half corresponding to asymmetric buckling (see Ref. 13). It is important to note that the asymmetric deformation propagated into the geometric imperfect section of the shell only after a time delay after impact. The deformation on impact was in the mode of the imperfection. The transfer of energy from the initial axisymmetric deformation to another (asymmetric) mode takes a finite length of time to complete due to radial inertia. Therefore buckling of perfect or axisymmetric imperfect cylinders on first passage of the pulse occurs in an axisymmetric mode for short time duration loading. These photoelastic results substantiate the analytical model used since the predicted modes were identical to those observed.

Similar high-speed photographs were taken for the asymmetric imperfect cylinder (AS1), again using the changing 22-½ deg isoclinic patterns as shown in Fig. 10. The deformation on impact was asymmetric, in the mode of the imperfection, for the full duration of loading. Table 2 presents a comparison of the measured mode wavelengths with those predicted using the buckling analysis.

Comparison of Buckling Loads

Dynamic buckling load predictions were based on vibrational strain amplitude vs input stress plots (such as Figs. 6-8) using the notion of a Southwell technique which was found to work very well in determining the asymptote, as can be seen in Fig. 11 for example. Both experimental and analytical buckling load predictions were obtained in this manner. Comparisons of buckling loads for different pulse durations are shown in Figs. 12-14.

Generally, the experimental data compare very well with the analytical curves. Furthermore, quantitatively, all experimental data, with the exception of shell model AS1 which was probably affected by truncation of the deflection function, lie within a few percent of the expected value, taking into account the anticipated displacement in the analytical curves due to the simple support end condition. However, all data including shell model AS1 showed qualitative agreement with the trend of the variation in buckling load with pulse-time duration. Thus, the buckling analysis adequately accounts for the principal mechanisms governing the radial deflections of the shell wall on collapse.

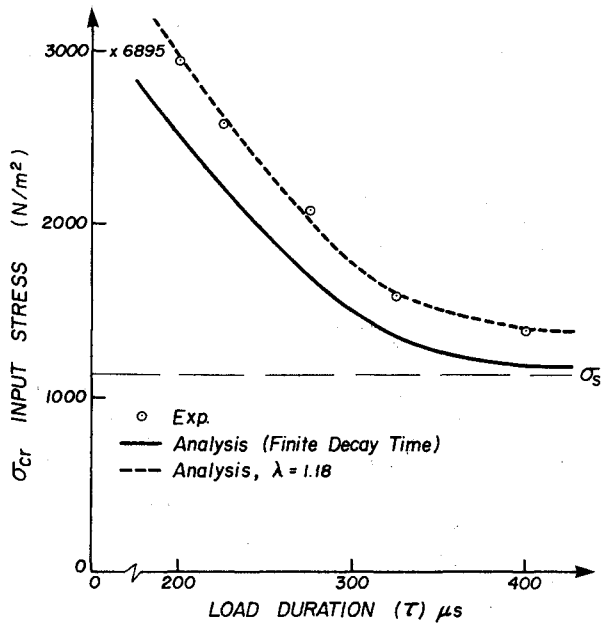

Fig. 14 Variation in buckling stress with load duration for shell AS1.

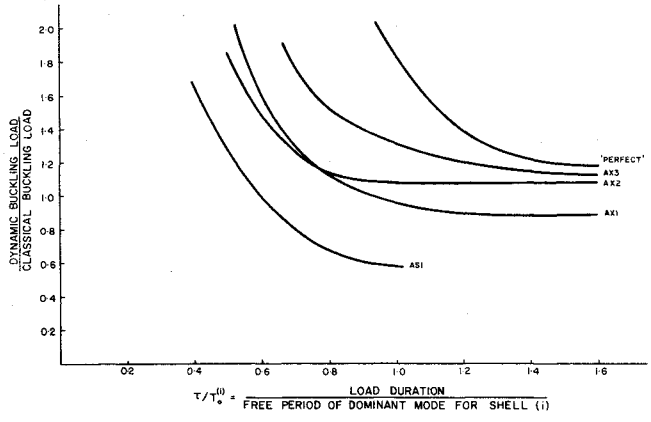

Fig. 15 Variation in theoretical buckling stress with load duration (experimental models).

Analytical curves are replotted in a more useful non-dimensional form shown in Fig. 15.

For time durations of loading less than the periods of free vibration, there was a very dramatic increase in the buckling stress due to the effect of radial inertia. It would appear that once the "knee" of this curve is defined, dynamic buckling for shorter pulse durations becomes a "material" rather than structural problem. In the time domain presently considered, there was also an increase in dynamic buckling load above static for the longest pulse durations for even very imperfect structures. (The static buckling load expressed as a fraction of the classical load for a similar "geometrically perfect" structure is given in Table 1 for all models.) This behavior differs from that of dynamic buckling of struts and several dynamic shell analyses[2,3] predicting that for time durations longer than the period of free vibration, imperfect structures buckle at loads below the static buckling value. Two factors are important in this discussion. First, due to the multiple modes possible for a shell during deformation, it is possible to excite more than one mode. In fact, it would seem that a minimum number is two; the free radial expansion (breathing) mode and at least one buckling or prebuckling mode. The requirement of zero kinetic energy at buckling imposed by the previously mentioned analyses is therefore too restrictive. Also, as was the case for most of the shell models of this study, the dynamic buckling mode may be time dependent.

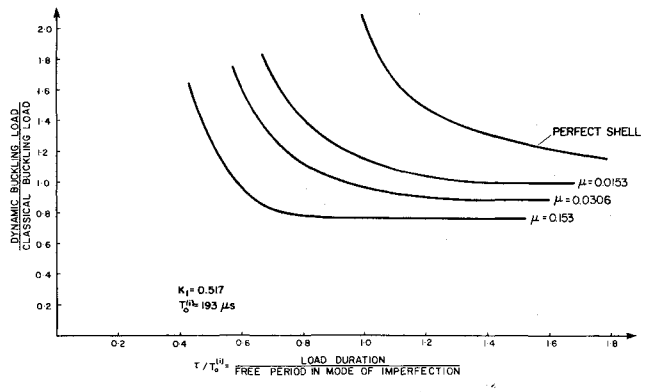

Fig. 16 Variation in dynamic buckling stress with imperfection amplitude (axisymmetric imperfection near critical wavelength).

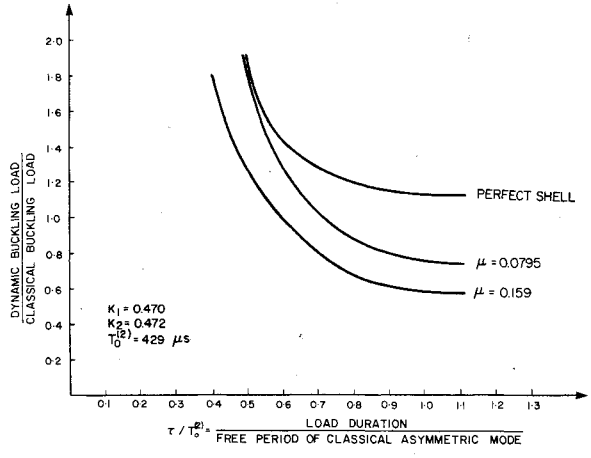

Fig. 17 Variation in dynamic buckling stress with imperfection amplitude (axisymmetric imperfection near critical wavelength).

High-speed photography has shown "geometrically perfect" and axisymmetric imperfect models buckle in a mode other than the static one in this time domain. Due to radial inertia, it is possible to drive the loading past a (static) bifurcation point if the time duration of loading is short. Of course, if the load is held long enough to exchange energy from one mode to another, the shell will buckle for any value of load above the static bifurcation point. Similarly, any load of "very long" duration cannot exceed the static value.

Although a limited number of axisymmetric imperfection parameters were considered, it would appear that the critical static axisymmetric imperfection wavelength was also the most degrading under dynamic loading.

It is possible then to predict minimum dynamic buckling loads as a function of pulse duration for an axisymmetric imperfection of given amplitude using the critical value. In addition to decreasing the load-carrying capability of the structure, increasing imperfection amplitude also shifts the "knee" of the dynamic buckling load curve to lower pulse duration values, as shown in Fig. 16. This effect can be shown analytically[13] to be due to the load dependence of the vibrational frequency. Consequently, the time domain in which dynamic buckling is possible is increased. Similar curves for an asymmetric imperfection of increasing amplitude near the static critical value can also be obtained (see Fig. 17). Although it has been shown that the analysis provided a conservative estimate for the asymmetric imperfect model, dynamic buckling loads for the shell containing the most degrading axisymmetric imperfection are above those of the model with the most degrading asymmetric imperfection of similar amplitude in this time domain. Furthermore, the dynamic buckling modes of the axisymmetric imperfect shell were shown to be different than the static case, whereas both

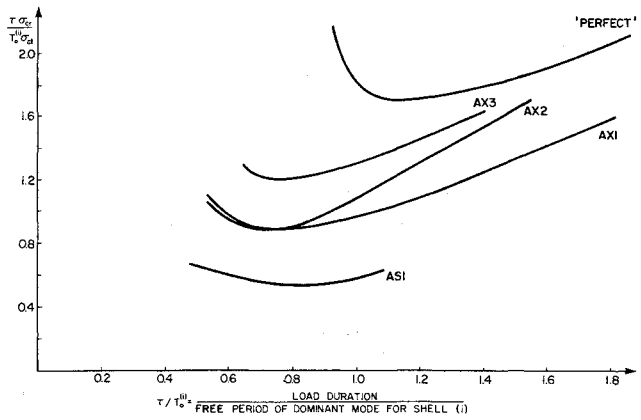

Fig. 18 Finite-time buckling impulse (experimental models).

dynamic and static modes are similar for the asymmetric imperfect shell. Transformation from one mode to another will occur with time resulting in a lower load-carrying capability for the axisymmetric imperfect shell for long pulse durations. However, for short time durations of loading, it would appear that the most degrading asymmetric imperfection causes a slightly larger reduction in the dynamic buckling load than the most degrading axisymmetric imperfection of equivalent amplitude due to the effect of radial inertia on the buckling mode.

In the time domain investigated, a minimum buckling impulse occurred for a pulse duration comparable to the free vibration period as shown in Fig. 18. It is reasonable to assume that this minimum was an overall minimum. For very long pulse durations, the dynamic buckling stress was near the static value. Approximate zero-time impulse expressions are given in Ref. 3, which yield values several times larger than the minimum. For short duration impulse type loading, the minimum buckling impulse for a shell of given imperfection amplitude represents a conservative but reasonable design criterion.

V. Conclusions

Experimental data have been presented showing the dynamic response of thin-walled circular cylindrical shells (with and without controlled initial shape imperfections) to transient dynamic "square-pulse" loading of varying time duration. These results indicate that buckling stiffness increased dramatically for short durations of loading due to the shell inertia in the radial direction. For short time durations (less than the period of free vibration in the static buckling mode), the dynamic buckling stress was increased above static for even relatively imperfect models. However, the presence of initial geometric shape imperfections can lead to substantial reductions in the dynamic buckling stress particularly if their wavelengths are close to the classical buckling modes. In addition, increasing imperfection amplitude decreases the pulse duration for which dramatic increases in buckling strength could be expected. These two quantities, dynamic buckling load and pulse duration, can be combined as a finite-time buckling impulse to provide a conservative dynamic buckling design criterion. It was also observed that in the time domain investigated, the dynamic buckling modes differed from the classical static asymmetric mode, tending rather to be axisymmetric for some thin-walled cylinders.

Because of the good agreement obtained between experiment and analysis, it is concluded that the simplified analytical buckling model adequately accounts for the principal mechanisms governing the dynamic response of circular cylinders.

Acknowledgment

The authors wish to acknowledge the financial support of our shell mechanics research program by the National Research Council of Canada under Grant No. A2783.

References

[1] Roth, R. S. and Klosner, J. M., "Nonlinear Response of Cylindrical Shells with Initial Imperfections Subjected to Dynamic Axial Loads," AIAA Paper 64-76, New York, Jan. 1964.

[2] Budiansky, B. and Hutchinson, J. W., "Dynamic Buckling of Imperfection-Sensitive Structures," *Proceedings of the 11th International Congress of Applied Mechanics*, Munich, West Germany, 1964.

[3] Hutchinson, J. W. and Budiansky, B., "Dynamic Buckling Estimates," *AIAA Journal*, Vol. 4, March 1966, pp. 525-530.

[4] Shiau, A. C., Roth, R. S., and Soong, T. T., "Dynamic Buckling of Conical Shells with Imperfections," *AIAA Journal*, Vol. 12, June 1974, pp. 755-760.

[5] Lakshmikantham, C. and Tsui, T., "Dynamic Stability of Axially-Stiffened Imperfect Cylindrical Shells under Axial Step Loading," *AIAA Journal*, Vol. 12, Feb. 1974, pp. 163-169.

[6] Fisher, C. A. and Bert, C. W., "Dynamic Buckling of an Axially Compressed Cylindrical Shell with Discrete Rings and Stringers," *Transactions of ASME, Journal of Applied Mechanics*, Series E, Vol. 40, No. 3, Sept. 1973, pp. 736-740.

[7] Maymon, G. and Singer, J., "Dynamic Elastic Buckling of Stringer-Stiffened Cylindrical Shells under Axial Impact," *Israel Journal of Technology*, Vol. 9, No. 6, 1971.

[8] Tamura, Y. S. and Babcock, C. D., "Dynamic Stability of Cylindrical Shells under Step Loading," *Transactions of ASME, Journal of Applied Mechanics*, Series E, Vol. 42, March 1975, pp. 190-194.

[9] Coppa, A. P. and Nash, W. A., "Dynamic Buckling of Shell Structures Subject to Longitudinal Impact," ASD TDR 62-744, Dec. 1962.

[10] Florence, A. L. and Goodier, J. N., "Dynamic Plastic Buckling of Cylindrical Shells in Sustained Axial Compressive Flow," *Transactions of ASME, Journal of Applied Mechanics*, Series E, Vol. 35, No. 2, March 1968.

[11] Lindberg, H. E. and Herbert, R. E., "Dynamic Buckling of Thin Cylindrical Shells under Axial Impact," Poulter Research Labs. Tech. Rept. 001-65, Feb. 1965.

[12] Tulk, J. D., "Buckling of Circular Cylindrical Shells under Dynamically Applied Axial Loads," Univ. of Toronto Institute for Aerospace Studies, Rept. 160, June 1972.

[13] Zimcik, D. G., "Stability of Circular Cylindrical Shells under Transient Axial Impulsive Loading," Univ. of Toronto Institute for Aerospace Studies, Rept. 206, March 1976.

[14] Tennyson, R. C., "An Experimental Investigation of the Buckling of Circular Cylindrical Shells in Axial Compression Using the Photoelastic Technique," Univ. of Toronto Institute for Aerospace Studies, Rept. 102, Nov. 1964.

[15] Tennyson, R. C., Zimcik, D. G., and Tulk, J. D., "The Analysis of the Dynamic Response of Linear Viscoelastic Materials," Univ. of Toronto Institute for Aerospace Studies, Rept. 159, June 1972.

[16] Muggeridge, D. B, "The Effects of Initial Axisymmetric Shape Imperfections on the Buckling Behavior of Cylindrical Shells under Axial Compression," Univ. of Toronto Institute for Aerospace Studies," Rept. 148, Dec. 1969.